ISSN 0023-1584, Kinetics and Catalysis, 2012, Vol. 53, No. 4, pp. 511–520. © Pleiades Publishing, Ltd., 2012.
Original Russian Text © A.M. Ozerova, O.A. Bulavchenko, O.V. Komova, O.V. Netskina, V.I. Zaikovskii, G.V. Odegova, V.I. Simagina, 2012, published in Kinetika i Kataliz, 2012, Vol. 53, No. 4, pp. 534–544.

Cobalt Boride Catalysts for Hydrogen Storage Systems Based on NH_3BH_3 and $NaBH_4$

A. M. Ozerova, O. A. Bulavchenko, O. V. Komova, O. V. Netskina, V. I. Zaikovskii, G. V. Odegova, and V. I. Simagina

Boreskov Institute of Catalysis, Siberian Branch, Russian Academy of Sciences, Novosibirsk, 630090 Russia

e-mail: ozerova@catalysis.ru

Received October 28, 2011

Abstract—The catalytic activity of cobalt borides forming in situ under conditions of NH_3BH_3 and $NaBH_4$ hydrolysis have been investigated. The reaction properties of the catalysts depend on the nature of the hydride. According to high-temperature X-ray diffraction, thermal analysis, high-resolution transmission electron microscopy, IR spectroscopy, and chemical analysis data, the nature of the hydride determines the particle size, chemical composition, and crystallization properties of the cobalt borides.

DOI: 10.1134/S0023158412040088

In recent decades, amorphous metal borides have been objects of extensive studies owing to their unique electronic, magnetic, and catalytic properties. Particular attention has been attracted by cobalt borides, which are inexpensive yet efficient catalysts for selective hydrogenation, hydrodesulfurization, and reduction reactions and for sodium borohydride ($NaBH_4$) hydrolysis for obtaining hydrogen to be used in portable energy sources [1, 2].

Amorphous cobalt borides are commonly synthesized by reducing a cobalt salt in a $NaBH_4$ solution [3–8]. The cobalt borides forming in situ from water-soluble cobalt salts [9–11] and Co_3O_4 or $LiCoO_2$ [10, 12, 13] upon $NaBH_4$ hydrolysis show high catalytic activity. Initially, the cobalt compound undergoes reduction to yield a cobalt boride phase (reaction (I)), and the latter catalyzes the hydrolysis of the hydride (reaction (II):

$$2CoCl_2 + 4NaBH_4 + 9H_2O \rightarrow Co_2B + 4NaCl + 12.5H_2\uparrow + 3B(OH)_3, \quad (I)$$

$$NaBH_4 + 2H_2O \xrightarrow{Cat} NaBO_2 + 4H_2\uparrow. \quad (II)$$

The $CoCl_2 + NaBH_4$ system was studied in greatest detail; however, the nature of the resulting cobalt boride Co_xB is still incompletely understood. Freshly prepared cobalt borides are X-ray-amorphous [1, 3, 4, 6–8]. Their diffraction patterns show a low-informative broad reflection at $2\theta = 45° \pm 2°$ [1, 3, 7–9, 14], which may be the superposition of reflections from different cobalt borides (CoB, Co_2B, Co_3B) and cobalt metal Co^0 [3, 7]. Chemical analysis confirms the presence of boron in the samples. According to the literature, the Co : B molar ratio in cobalt borides varies between 1.5 : 1 and 18 : 1 [1]. XPS data demonstrate that the cobalt borides are in a near-metallic state, but there is interaction between cobalt and boron that partially shifts electron density from B to the vacant *d* orbital of Co^0 [1, 5, 12].

In recent years, researchers' attention has been attracted by the promising hydrogen production and storage system based on the catalytic hydrolysis of ammonia borane (NH_3BH_3) [15–17] at ambient temperature:

$$NH_3BH_3 + 2H_2O \xrightarrow{Cat} NH_4BO_2 + 3H_2\uparrow. \quad (III)$$

Cobalt boride is claimed to be an active catalyst for this process [18, 19]. There have been first publications on the formation of a catalytically active phase in the NH_3BH_3 hydrolysis medium [20–22]. However, information concerning the nature of the active cobalt-containing phase is controversial. The formation of both Co^0 nanoparticles [21] and Co_2B [20, 23] was reported. The effect of the nature of the boron-containing hydride (NH_3BH_3, $NaBH_4$) on the size of the resulting active cobalt particle is not absolutely clear. Some authors believe that NH_3BH_3 has a stabilizing effect, preventing the agglomeration of the resulting nanoparticles [21]. Others report that the cobalt particles forming in the NH_3BH_3 hydrolysis medium have a larger size (100–200 nm) [23] than the particles forming in the $NaBH_4$ hydrolysis medium.

Here, we report a comparative study of the reactivity of the cobalt borides forming in the NH_3BH_3 and $NaBH_4$ hydrolysis media, their physicochemical properties, and the specific features of their crystallization. This study was carried out using high-temperature X-ray diffraction, thermal analysis, high-resolution transmission electron microscopy (HRTEM), IR spectroscopy, and chemical analysis.

EXPERIMENTAL

Sample Preparation

Cobalt borides were synthesized in situ from $CoCl_2 \cdot 6H_2O$ (USSR State Standard GOST 4525-77) under NH_3BH_3 hydrolysis conditions (**Co_xB-AB** sample) or $NaBH_4$ hydrolysis conditions (**Co_xB-SH** sample). The cobalt salt was added to a 0.12 M solution of $NaBH_4$ (OAO AVIABOR, 98 wt %) or NH_3BH_3 (OAO AVIABOR, 99 wt %) at 40°C under continuous stirring. The hydride-to-$CoCl_2 \cdot 6H_2O$ molar ratio was 25 : 1. The volume of released hydrogen was measured with a gas burette. After the end of gas evolution, the resulting black precipitate was separated from the mother liquor using a magnet, thoroughly washed with acetone (USSR State Standard GOST 2603-79), and vacuum-dried at 70°C for 3 h. The product was stored in an Ar atmosphere. The Co_2B/Co_3O_4 sample was obtained in a similar way by carrying out $NaBH_4$ hydrolysis in the presence of Co_3O_4 (USSR State Standard GOST 4467-79). The preparation and characterization of Co_2B/Co_3O_4 was described in detail in an earlier publication [13].

The catalytic activity of the synthesized cobalt borides was studied at 40°C in a temperature-controlled, stirred-tank, glass reactor, with a magnetic stirrer rotating at a speed of 800 rpm. The catalysts were undried cobalt borides synthesized in situ by adding a freshly prepared aqueous solution of $NaBH_4$ or NH_3BH_3 (1.2 mmol, 10 mL) to $CoCl_2 \cdot 6H_2O$ (0.0117 g). The volume of hydrogen released was measured with a 100-mL gas burette and was corrected to N.T.P. In stability tests for the Co_xB-SH sample, the catalyst was separated from the reaction medium after the conversion of the first portion of the hydride and was washed with distilled water, and another portion of the hydride was then added.

The hydrogen generation rate was calculated as

$$W = \frac{V_{H_2}}{t_{1/2} m_{Co}},$$

where W is the reaction rate (mL s^{-1} g^{-1}), V_{H_2} is the volume of released hydrogen (mL) corrected to N.T.P., $t_{1/2}$ is the time (s) at which the volume of released H_2 is 50 mL, and m_{Co} is the mass of cobalt in the catalyst (g) determined by chemical analysis.

Sample Characterization

The cobalt and boron contents of the samples were determined by ICP-AES on an Optima 4300V spectrometer (Germany).

HRTEM images were obtained on a JEM-2010 microscope (accelerating voltage of 200 kV, resolution of 0.14 nm). The images were analyzed and filtered using the DigitalMicrograph program (GATAN). Elemental analysis of the samples was carried out by energy-dispersive X-ray microanalysis (EDX) on an EDAX Phoenix spectrometer equipped with a Si(Li) detector with an energy resolution of 130 eV or higher. The samples to be analyzed were applied to a holey carbon film mounted on a standard copper grid.

IR spectra were recorded as CsI pellets in air at room temperature on an MB-102 (Bomem) Fourier-transform spectrometer.

Thermal analysis was carried out on an STA 449 C Jupiter® system in flowing helium (10 mL/min) between 25 and 600°C at a heating rate of 2.5, 5, 10, or 15 K/min. The activation energy of crystallization was determined by the Kissinger method [24] using the equation

$$\ln\left(\frac{T_{max}^2}{\beta}\right) = \frac{E_a}{RT} + C,$$

where β is the heating rate, T_{max} is the exothermic peak temperature, E_a is the activation energy of crystallization, R is the gas constant, and C is a constant. The plot of $\ln(T_{max}^2/\beta)$ versus $1/T$ was a straight line, and, from its slope, we derived the E_a value.

High-temperature diffraction patterns were recorded in air and in vacuo on a D8 diffractometer (Bruker, Germany) using CuK_α radiation and a high-temperature X-ray chamber (Anton Paar, Austria). The diffractometer was fitted with a Gebel mirror (Germany) producing a parallel X-ray beam. Vacuum X-ray diffraction was performed at a residual pressure of 5×10^{-6} bar. Diffraction patterns were recorded in the 15°–70° range with 0.05° increments and a counting time of 5–20 s per point. The sample heating rate was 10 K/min. The reflections from Pt metal present in the diffraction patterns arise from the platinum substrate. In one case, the Co_xB-AB sample was calcined at 500°C for 3 h in an Ar atmosphere. The particle (crystallite) size was calculated from the 111 reflection for Co and from the 103 reflection for Co_3B using the Scherrer formula. In these calculations, the physical line broadening characteristic of the Bruker diffractometer (0.07°) was subtracted from the observed line width. The crystallite size calculation error was 10%.

RESULTS AND DISCUSSION

Figure 1 plots the volume of released hydrogen versus time upon contact of the cobalt chloride with $NaBH_4$ and NH_3BH_3 solution. The $CoCl_2 + NaBH_4$ system is characterized by a high initial hydrogen generation rate, while the system involving NH_3BH_3, which is a milder reductant than $NaBH_4$, shows an induction period at the early stages of the reaction. It was demonstrated earlier that the induction period is determined by the time required for the reduction of the cobalt compound to an active cobalt-containing phase [10, 13]. The formation of an active component in situ is followed by the catalytic hydrolysis of the hydride, which is accompanied by vigorous hydrogen evolution. After the end of gas evolution, the catalyst was separated from the reaction medium, washed with

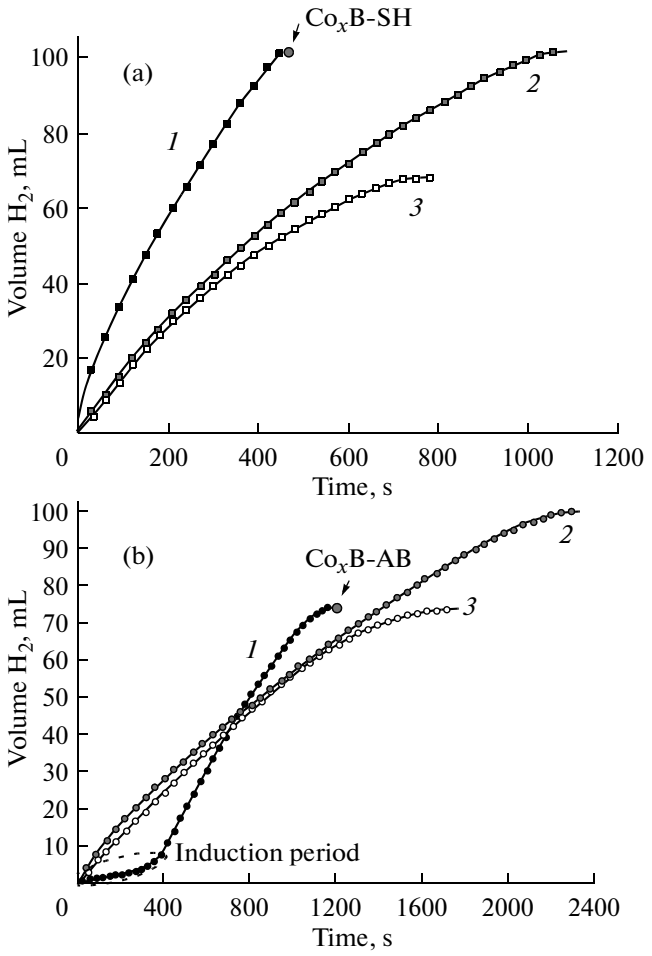

Fig. 1. (a) Hydrogen evolution (*1*) in the synthesis of Co_xB-SH and (*2, 3*) in the testing of this sample in (*2*) $NaBH_4$ and (*3*) NH_3BH_3 hydrolysis. (b) Hydrogen evolution (*1*) in the synthesis of Co_xB-AB and (*2, 3*) in the testing of this sample in (*2*) $NaBH_4$ and (*3*) NH_3BH_3 hydrolysis.

distilled water in the reactor, and reused in $NaBH_4$ and NH_3BH_3 hydrolysis (Fig. 1). Clearly, the hydrogen generation rate is practically independent of the nature of the hydride and is determined by the properties of the catalyst. The Co_xB-SH sample, which was obtained from $CoCl_2$ in the $NaBH_4$ medium, is catalytically more active than Co_xB-AB, which was formed in the NH_3BH_3 medium. Use of Co_xB-SH, the most active composition, in H_2 generation via $NaBH_4$ hydrolysis demonstrated (Fig. 2) that the hydrogen evolution rate decreases by approximately 35% over the first five testing cycles and then stabilizes and remains invariable for at least 11 subsequent cycles. The hydrogen yield was always near 100% (Fig. 2). The decline of the activity of the catalyst may be due to the aggregation of cobalt-containing particles and the adsorption of reaction products on their surface [25, 26]. In order to elucidate the cause of the high activity of Co_xB-SH, we studied its physicochemical

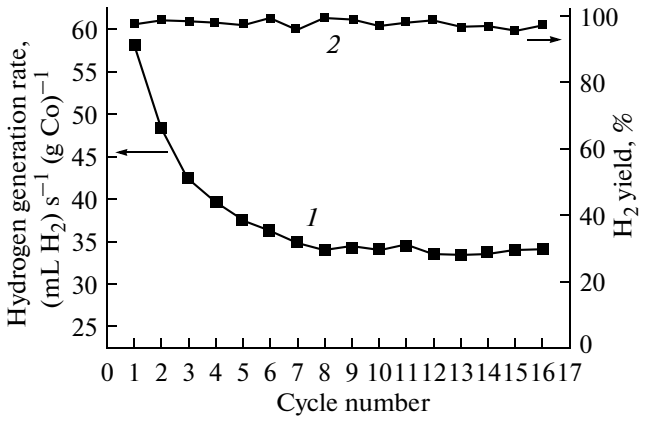

Fig. 2. Hydrogen (*1*) generation rate and (*2*) yield in the cyclic tests of the Co_xB-SH catalyst in $NaBH_4$ hydrolysis.

properties and compared them with the properties of the less active catalyst Co_xB-AB.

There have been many reports dealing with cobalt borides synthesized by cobalt salt reduction in a $NaBH_4$ solution. The nature of these borides is still not fully understood. However, the common opinion is that the cobalt borides consist of a cobalt-containing core surrounded by a shell of oxygen-containing compounds of cobalt and boron [1, 9]. The formation of this shell is due to the oxidation of the cobalt borides in the aqueous medium [1]. As was demonstrated above, the compounds resulting from the action of an NH_3BH_3 solution on Co^{2+} have been studied to a lesser extent.

Our Co_xB-AB and Co_xB-SH samples were X-ray-amorphous, ferromagnetic, gray and black powders, respectively. The cobalt and boron contents of the samples were determined by chemical analysis. The Co_xB-SH sample contained 81.7 wt % Co and 7.4 wt % B. The total percentage of Co and B is below 100%. The remaining 10.9 wt % is likely due to oxygen. The presence of oxygen in similar samples was discussed by other authors [6, 9]. The Co : B : O molar ratio in Co_xB-SH was calculated to be 2.0 : 1.0 : 1.0. Note that cobalt boride with the Co : B = 2 : 1 stoichiometry usually forms when $CoCl_2$ and $NaBH_4$ are used as the initial reactants [1, 6–9]. According to chemical analysis data, Co_xB-AB contained 94.3 wt % Co and 5.7 wt % B, implying a molar ratio of Co : B : O = 3.0 : 1.0 : 0.

IR spectroscopic data also indicate that the samples are different. The IR spectra of both Co_xB-SH and Co_xB-AB show structureless absorption in the 4000–400 cm^{-1} range (Fig. 3). The absorption bands at 3475 and 1635 cm^{-1} are due to O–H stretching and H–O–H bending vibrations, respectively, indicating that the samples contain small amounts of water. The IR spectrum of Co_xB-SH additionally shows absorption bands at 1390, 1060, 850, and 688 cm^{-1}, which are characteristic of B–O vibrations [27]. The pres-

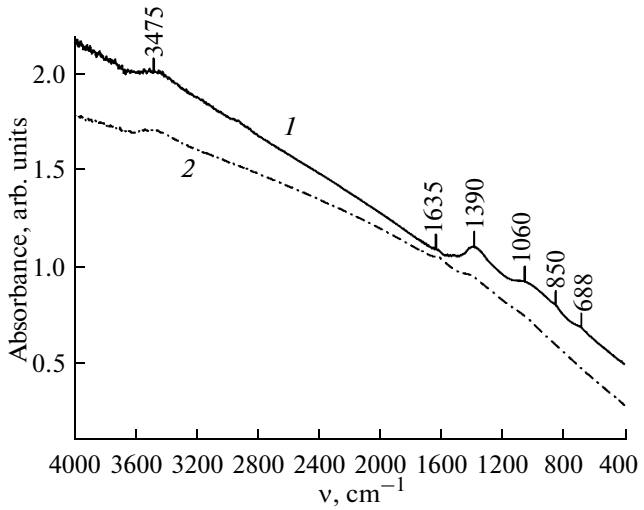

Fig. 3. IR spectra of (*1*) Co_xB-SH and (*2*) Co_xB-AB.

ence of these bands is evidence that Co_xB-SH, as distinct from Co_xB-AB, contains compounds having B–O bonds. These oxygen-containing boron compounds are conventionally viewed as borate anions and boron oxides adsorbed on the surface [1, 5, 28]. Under certain conditions, the synthesis of cobalt borides in solution may yield amorphous cobalt borate as a by-product [8, 9, 29].

The TEM examination of the samples (Fig. 4) demonstrated that the particle size of the cobalt borides Co_xB-SH and Co_xB-AB depends on the nature of the hydride used as the reductant in their synthesis. The boride Co_xB-AB consists of aggregated globular particles 150–500 nm in diameter, with a dominant diameter of about 150 nm, while Co_xB-SH consists of smaller particles 20–60 nm in diameter, with a dominant diameter of about 30 nm (Figs. 4a, 4b). A characteristic feature of the globular particles of Co_xB-SH is the presence of block intergrowth boundaries, which can be seen as short light strokes in the TEM images of sample (Fig. 4e).

The EDX spectra of the near-surface zones of cobalt boride particles in Co_xB-SH and Co_xB-AB indicate that these particles contain boron and oxygen along with cobalt. The relative amount of oxygen in Co_xB-SH is larger than in Co_xB-AB. This is in agreement with the chemical analysis and IR spectroscopic data. Boron in these samples was difficult to quantify because of the limited sensitivity of the device to this element.

The cobalt boride particles in the samples are coated by a 2- to 3-nm-thick shell (Figs. 4d–4f). The HRTEM images (Figs. 4d, 4f) show small, ~2-nm crystalline particles included in this shell. The interplanar spacings in the lattice of these crystallites are assignable both to Co metal and to cobalt oxides (Co_3O_4 and CoO). The reflections in the inset in Fig. 4d correspond to the interplanar spacing $d_{100} = 0.22$ nm in hexagonal Co, while Fig. 4f displays the lattice of CoO or Co_3O_4 ($d = 0.24$ and 0.47 nm). The crystallites on the cobalt boride surface are stabilized by carbon, which possibly comes from acetone used to wash the samples. Traces of carbon are also indicated by the EDX spectra (Fig. 4c). According to the literature, the shell of the particles may consists of amorphous oxide compounds of boron [6] and cobalt [30] and a Co–B–O phase [9]. It is likely that, as Co_xB-SH and Co_xB-AB are examined under an electron microscope, the shell undergoes destruction to yield small crystallites of cobalt oxides or cobalt metal, the latter resulting from the reducing action of the electron beam.

The inset in Fig. 4f presents a Fourier-filtered HRTEM image of a cobalt boride particle in the Co_xB-SH sample. According to widespread views [1, 3, 4, 6–9], the borides obtained in a $NaBH_4$ medium are X-ray-amorphous. The image presented in Fig. 4f indicates the cobalt boride structure is partially ordered within ~1-nm areas. The interplanar spacing derived from this image is 0.24 nm. However, because of the pronounced irregularity of the structure, it is problematic to assign this interplanar spacing to any particular phase. It is possible that this spacing corresponds to the disordered Co_3B phase. Obviously, the small crystallite size in this structure does not allow any indication of structural ordering to be detected by X-ray diffraction. It is difficult to study the Co_xB-AB sample in this way because of the large size of its particles.

Thus, the two synthesized cobalt boride samples differ in their Co : B ratio, particle size, and degree of oxidation. The particles of Co_xB-SH are smaller than the particles of Co_xB-AB and are oxidized to a larger extent. The low oxygen content of Co_xB-AB is due to the fact that the particles of this sample are larger by a factor of several tens. This can apparently be explained by the lower rate of their formation (Fig. 1), since NH_3BH_3 is known to be a milder reductant than $NaBH_4$.

Amorphous phases are commonly characterized by investigating their crystallization, which depends on the state of the initial phase. Thermal analysis of amorphous cobalt borides enables one to observe heat evolution due to crystallization. Figures 5a and 5b show the DTA figures of Co_xB-SH and Co_xB-AB, respectively, recorded at different heating rates (2.5 to 15 K/min). Both figures indicate an exotherm with a peak temperature of $T_{max} = 444$–487°C. This exotherm is assigned either to the crystallization of amorphous cobalt boride [14, 23] or to the conversion of cobalt boride into cobalt metal [9]. The activation energy of the phase transition was calculated by the Kissinger method to be 541 and 355 kJ/mol for Co_xB-SH and Co_xB-AB, respectively (Fig. 5c). Note that, at equal heating rates, T_{max} for Co_xB-AB is lower than T_{max} for Co_xB-SH, although samples with a larger particle size (see Fig. 4) are usually characterized by larger

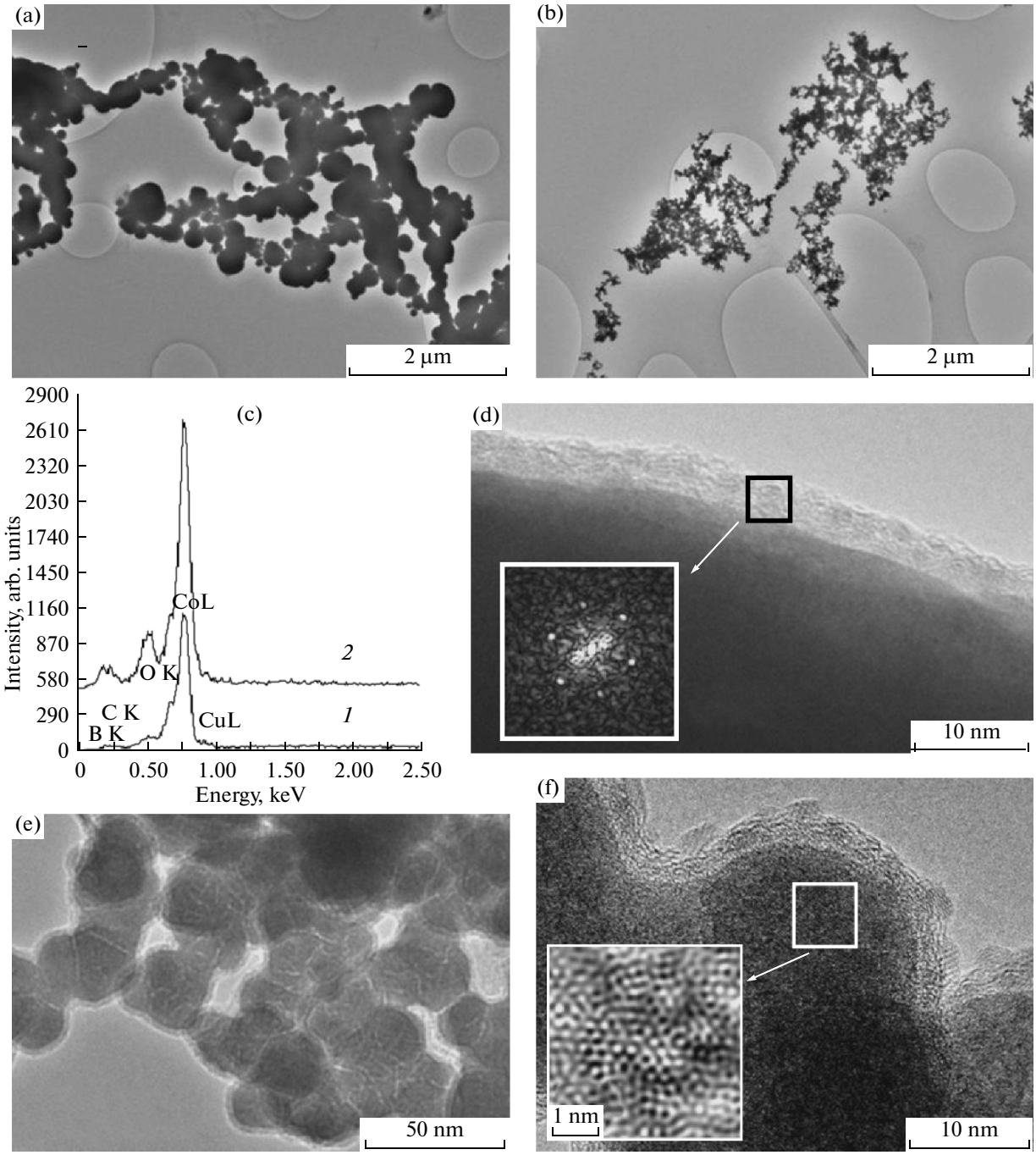

Fig. 4. TEM images and EDX spectra of the two cobalt boride samples: (a, b) morphology of Co_xB-AB and Co_xB-SH particles, respectively; (c) EDX spectra of (*1*) Co_xB-AB and (*2*) Co_xB-SH; (d) HRTEM image of the near-surface zone of a Co_xB-AB particle coated with a shell (inset: SAED pattern of a particle from the shell, which can be assigned to the hexagonal cobalt with $d_{100} = 0.22$ nm); (e) TEM image of a Co_xB-SH particle with a shell; (f) HRTEM image of the Co_xB-SH sample (inset: Fourier-filtered image of an area with a partially ordered structure).

T_{max} values [31]. This uncommon observation in our experiments might be due to the amorphous phases being in different states and having their own specific features of crystallization.

There have been reports on the crystallization of amorphous cobalt borides into various products. For example, calcination of cobalt borides at 500°C in flowing Ar [8, 20, 23] or N_2 [4, 14, 32) or in vacuo [7] was reported to yield the Co^0-containing CoB phase [4], Co_2B [8, 23], a mixture of the Co_2B and Co_3B phases [32], $Co^0 + Co_2B$ [7, 20], and $Co^0 + Co_2B + Co_3B$ [14]. Unfortunately, insufficient attention has

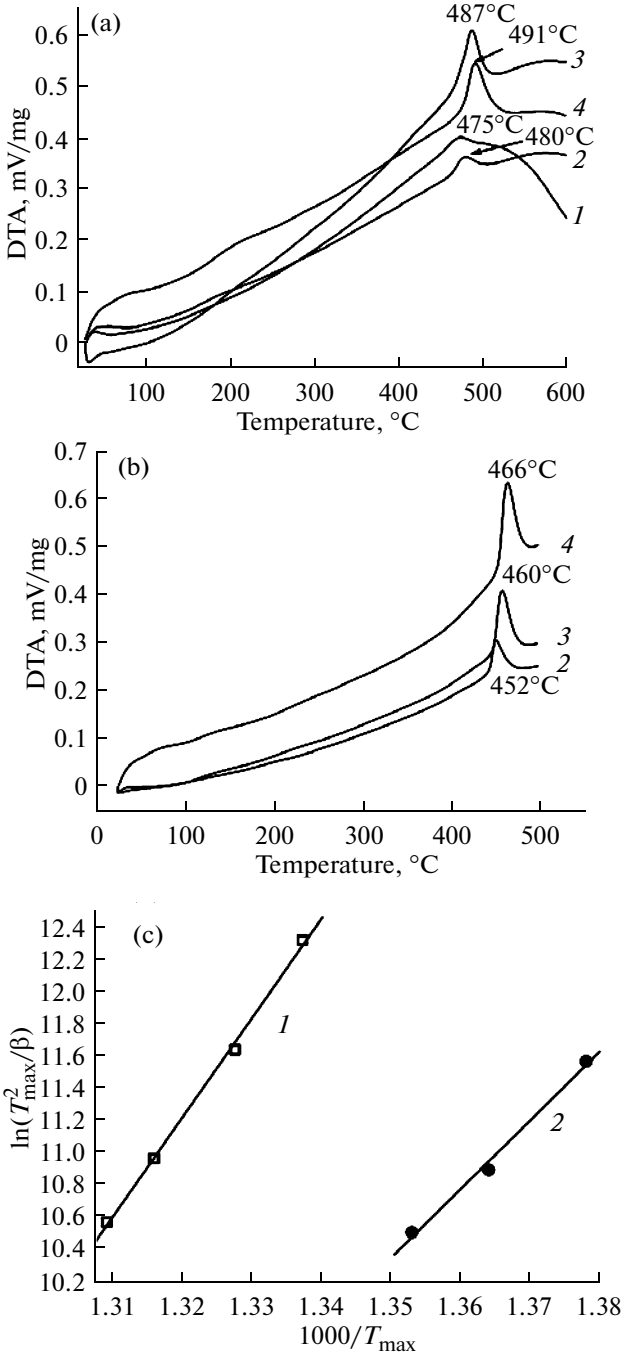

Fig. 5. DTA profiles of (a) Co_xB-SH and (b) Co_xB-AB recorded at a heating rate of (*1*) 2.5, (*2*) 5, (*3*) 10, and (*4*) 15 K/min. (c) Kissinger plots for (*1*) Co_xB-SH and (*2*) Co_xB-AB.

been paid to explaining this diversity of crystalline phase. It is believed that this multitude of phases arises from the variation of Co_xB synthesis and heat treatment conditions [1]. Probably, the key factor here is the boron content of the initial cobalt boride sample [33]. The dominant crystalline phase in the systems with a low boron content (Co : B > 4.5 mol/mol) is Co^0. As the boron content is increased, the crystallization of a cobalt boride (Co_2B, Co_3B) as the main phase becomes more likely. In reports dealing with the crystallization of amorphous cobalt borides, it is noted that, at moderate temperatures of up to 450°C, the main crystallizing phases are Co^0 (fcc) and Co_3B [6, 34–36]. As the temperature is further raised, these phases may undergo interconversions. It was demonstrated [8] that the formation of the metallic phase Co^0 upon heat treatment of cobalt borides may be due to their oxidation by atmospheric oxygen and to the following redox reaction between Co_xB and cobalt borate $Co(BO_2)_2$:

$$2Co_2B + Co(BO_2)_2 \rightarrow 5Co + B_2O_x. \qquad \text{(IV)}$$

As was mentioned above, the formation of cobalt borate along with cobalt boride can take place via the interaction of cobalt compounds with $NaBH_4$ in aqueous solution [8, 9, 29].

In order to obviate the need for taking into account the effect of oxygen-containing phases on the crystallization of amorphous cobalt borides, we will initially consider the high-temperature X-ray diffraction data for the Co_xB-AB sample with Co : B = 3 : 1 mol/mol and traces of oxygen (Fig. 6). From room temperature to 500°C, Co_xB-AB is X-ray-amorphous. Its diffraction patterns contain a broad line at $2\theta = 40°–53°$, which is conventionally assigned to amorphous cobalt borides [1, 3, 7–9, 14]. At 500°C, the sample begins to crystallize into the cobalt boride Co_3B and cobalt metal (fcc) phases, whose crystallite sizes are listed in the table. These data are in agreement with the literature [34–36]. As the calcination temperature is raised, the proportion of Co^0 increases, the proportion of the Co_3B phase decreases, and the particles grow larger through sintering (table). At 700°C, Co_3B turns entirely into the cobalt metal phase Co^0. Note that this conversion is fairly frequently observed in cobalt boride systems as the temperature is elevated to 700°C [1, 4, 6, 9]. The Co_3B phase can disappear via disproportionation [34–36]. The proportion of cobalt metal increases not only as the calcination temperature is increased, but also as the time for which the sample is held at a lower temperature is extended (Fig. 6b).

X-ray diffraction data for the Co_xB-SH with a Co : B : O molar ratio of 2 : 1 : 1 are presented in Fig. 7a. The crystallization of this sample is observed at a higher temperature (600°C) than the crystallization of Co_xB-AB. This is in agreement with the DTA data indicating that the former sample crystallizes with a higher activation energy. No crystalline cobalt boride phases form in Co_xB-SH, although this sample is richer in boron than Co_xB-AB and, accordingly, the probability of boride crystallization in this sample is higher [33]. The diffraction pattern presented in Fig. 7a shows reflections from only cobalt metal Co^0 (fcc). Raising the temperature to 700°C causes the crystallization of the entire sample into Co^0, as is indicated by the disappearance of the halo in the 40°–53° range.

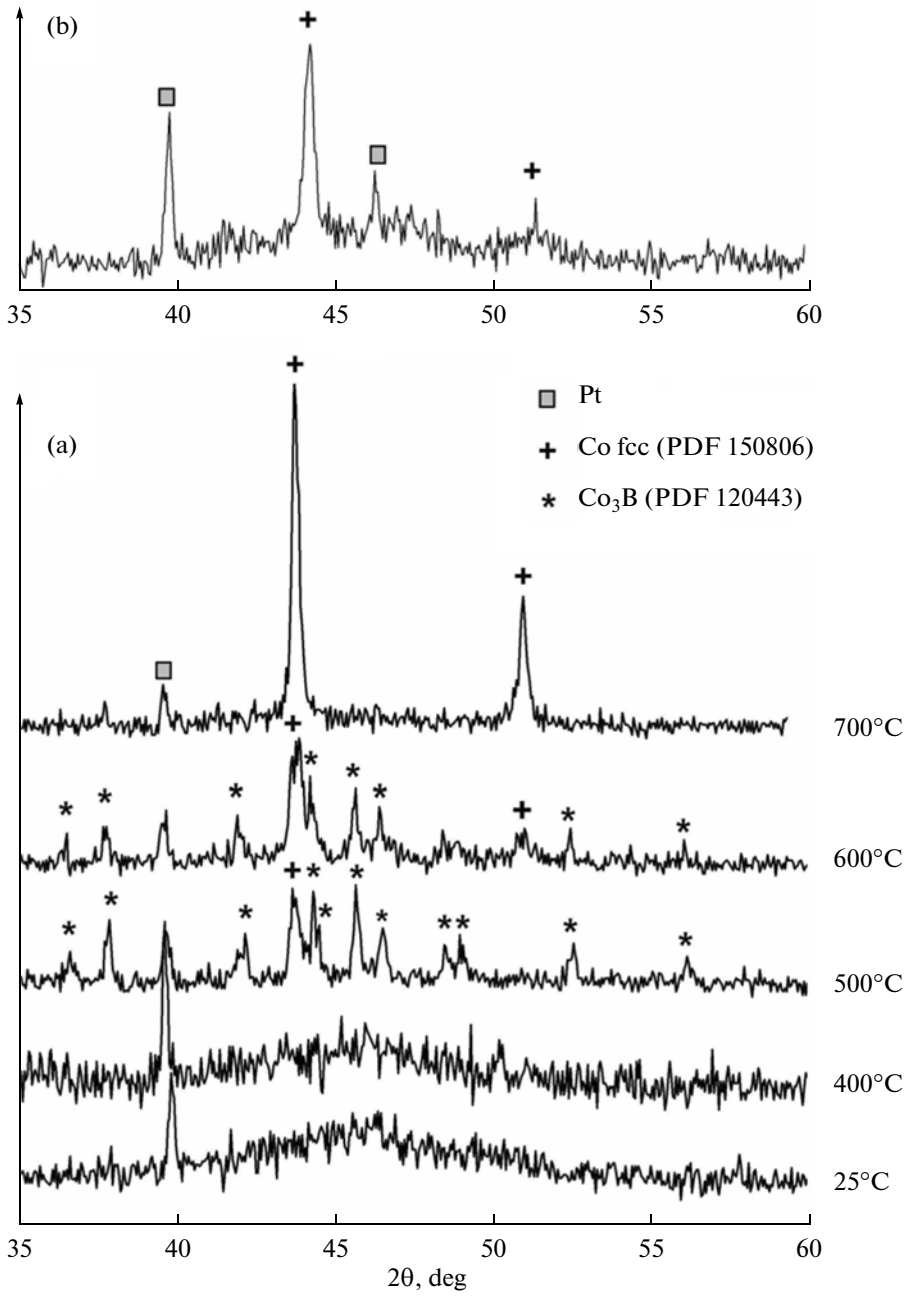

Fig. 6. X-ray diffraction patterns of Co_xB-AB recorded (a) at 25°C and after calcination at 400, 500, 600, and 700°C in vacuo and (b) after calcination at 500°C in Ar for 3 h.

This finding can be explained by the presence of oxygen in the sample and by the decrease in the boron content of the cobalt boride phase as a consequence of borate formation, which is confirmed by IR spectroscopic data. Our calculations demonstrated that the amount of oxygen present in the sample is sufficient for the oxidation of the boride particles to cobalt metal via reaction (IV). Heat treatment in the presence of atmospheric air rapidly yields of fine Co^0 particles (6.5 nm; see the table) even at 400°C (Fig. 7b).

The effect of oxygen on the crystallization processes was also observed in a study of Co_2B/Co_3O_4 obtained by Co_3O_4 reduction in a $NaBH_4$ solution [13]. This sample was thoroughly characterized by chemical analysis, IR spectroscopy, TEM, X-ray diffraction, and magnetic susceptibility measurements in our earlier study [13]. According to [13], this sample was a mixture of an ultrafine amorphous Co_2B phase with a mean particle size of 30 nm and partially reduced initial cobalt oxide Co_3O_4. At room tempera-

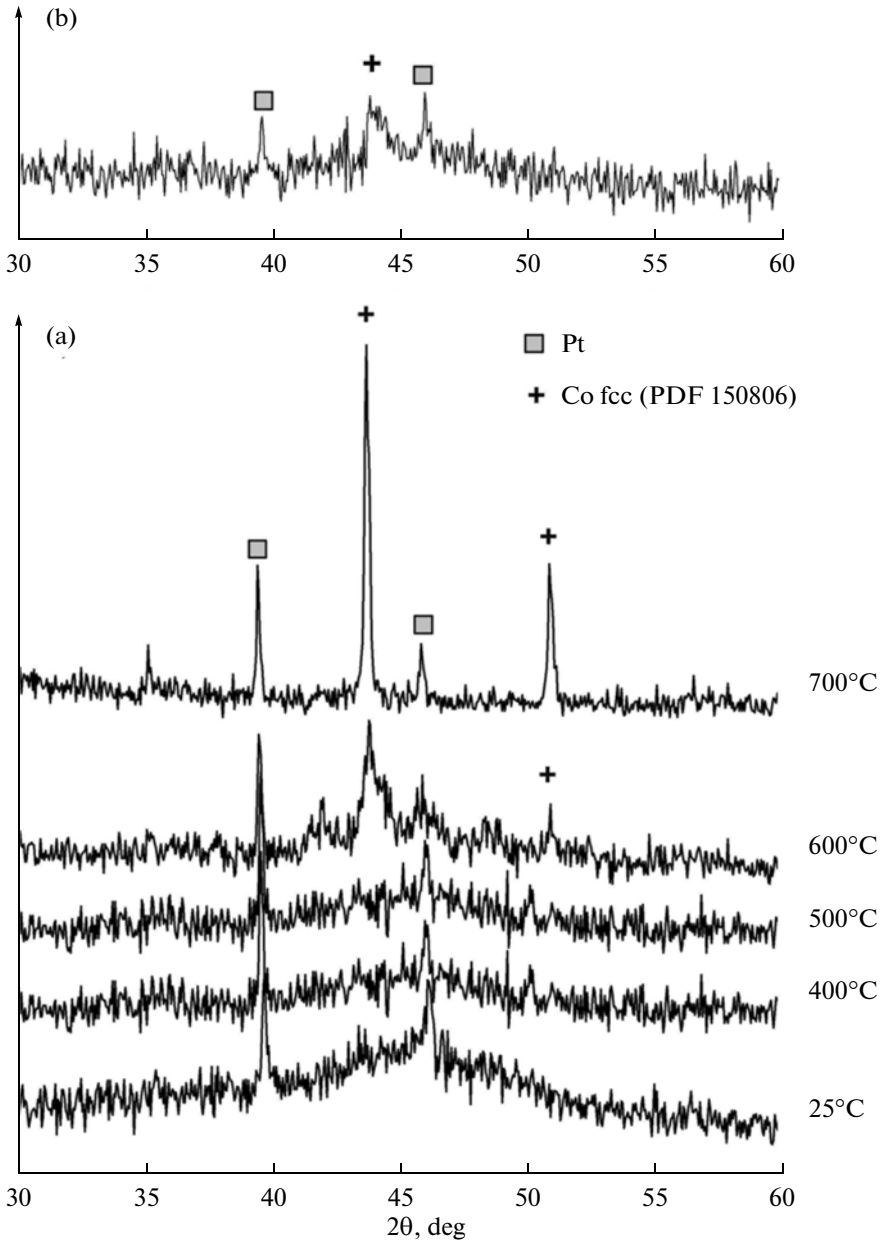

Fig. 7. X-ray diffraction patterns of Co_xB-SH recorded (a) at 25°C and after calcination at 400, 500, 600, and 700°C in vacuo and (b) after calcination at 400°C in air.

ture, the X-ray diffraction pattern of Co_2B/Co_3O_4 (Fig. 8) is consistent with the structure of the initial Co_3O_4. In the $2\theta = 40°–47°$ range, there is a broad peak characteristic of amorphous cobalt borides [1, 3, 7–9, 14]. Heat treatment of Co_2B/Co_3O_4 at 500–600°C results in the formation of crystalline phases of CoO and Co^0 with a particle size of 38 nm (600°C). A special-purpose experiment demonstrated that the formation of the CoO phase is due to Co_3O_4 reduction upon heating in vacuo (Fig. 8). Thus, the calcination of amorphous Co_2B mixed with cobalt oxides yielded only the Co^0 phase, and no crystalline cobalt boride phases were observed. These data are in agreement with our results and with data of other authors [8]. Heat treatment of the amorphous cobalt borides in the presence of oxygen-containing compounds or gaseous oxygen results in the oxidation of the borides to Co^0. Therefore, the oxygen-containing phases play a significant role in the crystallization of amorphous cobalt borides and have an effect on the composition of the crystalline products.

Crystallite size data for the phases resulting from progressive heating of Co_xB-AB and Co_xB-SH at a rate of 10 K/min

Sample	Calcination conditions	Phase	Crystallite size, nm
Co_xB-AB	500°C, vacuum	Co_3B	74
		Co	27
	600°C, vacuum	Co_3B	87
		Co	22
	700°C, vacuum	Co	63
	500°C, Ar, 3 h*	Co	37
Co_xB-SH	600°C, vacuum	Co	10
	700°C, vacuum	Co	79
	400°C, air	Co	6.5

* The X-ray diffraction pattern was recorded at room temperature.

Thus, the catalytic properties of the cobalt compounds in $NaBH_4$ and NH_3BH_3 hydrolysis are due to their reduction in the reaction medium to a catalytically active cobalt boride phase. We have established that the nature of the hydride determines the reactivity and physicochemical properties of the cobalt borides forming in situ. The interaction between the water-soluble cobalt salt $CoCl_2$ and an NH_3BH_3 solution yields an amorphous cobalt boride phase with Co : B = 3 : 1 mol/mol. The low reducing power of NH_3BH_3 is favorable for the formation of large, 150- to 500-nm boride particles containing traces of oxygen-containing compounds. Use of $NaBH_4$, a stronger reductant, ensures the instantaneous formation of cobalt boride with a smaller particles size of 20–60 nm and a larger degree of oxidation (Co : B : O = 2 : 1 : 1). According to HRTEM data, the resulting particles have a partially ordered structure within a ~1-nm region. This cobalt boride is catalytically more active than the cobalt boride obtained in the NH_3BH_3 medium. Apparently, the small particle size and the presence of oxygen-containing compounds reducible to a catalytic phase under the action of the hydride are the factors that make this sample catalytically more active. Earlier, we observed that Co_3O_4, CoO, and cobalt borate are very active in $NaBH_4$ hydrolysis [13, 29].

The study of the amorphous cobalt borides has demonstrated that oxygen and oxygen-containing compounds exert a significant effect on boride crystallization. The crystalline Co_3B phase forms only in the sample obtained in the ammonia borane medium. Probably, owing to the presence of oxygen in the ultrafine particles resulting from the in situ reduction of $CoCl_2$ and Co_3O_4 with sodium borohydride, cobalt boride in these particles undergoes oxidation to cobalt metal upon heating.

ACKNOWLEDGMENTS

This work was supported by the Russian Foundation for Basic Research (grant no. 09-08-00505a).

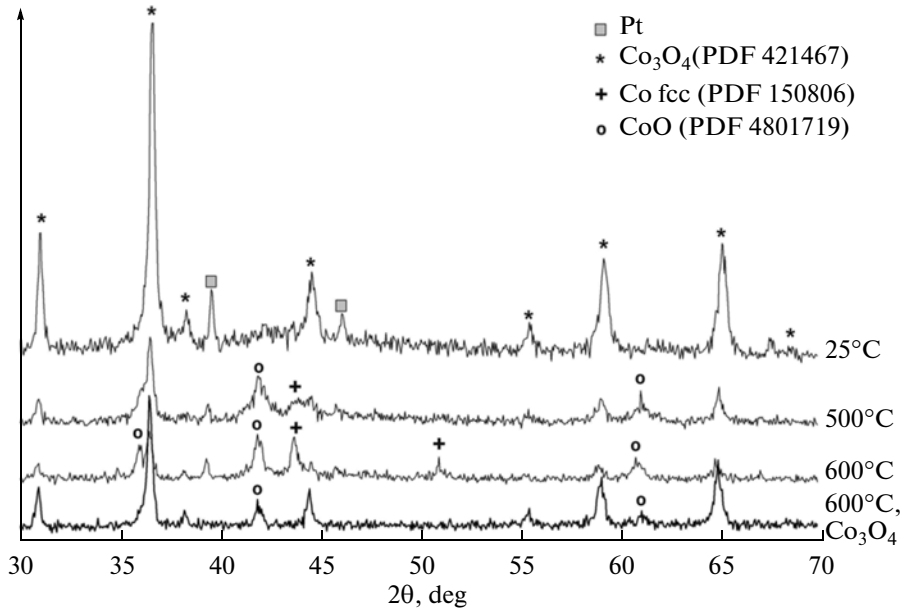

Fig. 8. X-ray diffraction patterns of Co_2B/Co_3O_4 recorded at 25°C and after calcination at 500 and 600°C in vacuo; X-ray diffraction pattern of Co_3O_4 calcined at 600°C in vacuo.

REFERENCES

1. Demirci, U.B. and Miele, P., *Phys. Chem. Chem. Phys.*, 2010, vol. 12, no. 44, p. 14651.
2. Demirci, U.B., Akdim, O., Andrieux, J., Hannauer, J., Chamoun, R., and Miele, P., *Fuel Cells*, 2010, vol. 10, no. 3, p. 335.
3. Jeong, S.U., Cho, E.A., Nam, S.W., Oh, I.H., Jung, U.H., and Kim, S.H., *Int. J. Hydrogen Energy*, 2007, vol. 32, no. 12, p. 1749.
4. Wu, C., Wu, F., Bai, Y., Yi, B., and Zhang, H., *Mater. Lett.*, 2005, vol. 59, nos. 14–15, p. 1748.
5. Patel, N., Guella, G., Kale, A., Miotello, A., Patton, B., Zanchetta, C., Mirenghi, L., and Rotolo, P., *Appl. Catal., A*, 2007, vol. 323, p. 18.
6. Corrias, A., Ennas, G., Licheri, G., Marongiu, G., and Paschina, G., *Chem. Mater.*, 1990, vol. 2, no. 4, p. 363.
7. Lu, J., Dreisinger, D.B., and Cooper, W.C., *Hydrometallurgy*, 1997, vol. 45, no. 3, p. 305.
8. Glavee, G.N., Klabunde, K.J., Sorensen, C.M., and Hadjipanayis, G.C., *Langmuir*, 1992, vol. 8, no. 3, p. 771.
9. Garron, A., Świerczyński, D., Bennici, S., and Auroux, A., *Int. J. Hydrogen Energy*, 2009, vol. 34, no. 3, p. 1185.
10. Komova, O.V., Simagina, V.I., Netskina, O.V., Kellerman, D.G., Odegova, G.V., Ishchenko, A.V., and Rudina, N.A., *Catal. Today*, 2008, vol. 138, nos. 3–4, p. 260.
11. Wu, C., Bai, Y., Wu, F., Yi, B.L., and Zhang, H.M., *Int. J. Hydrogen Energy*, 2010, vol. 35, no. 7, p. 2675.
12. Krishnan, P., Hsueh, K.L., and Yim, S.D., *Appl. Catal., B*, 2007, vol. 77, nos. 1–2, p. 206.
13. Simagina, V.I., Komova, O.V., Ozerova, A.M., Netskina, O.V., Odegova, G.V., Kellerman, D.G., Bulavchenko, O.A., and Ishchenko, A.V., *Appl. Catal. A*, 2011, vol. 394, nos. 1–2, p. 86.
14. Li, H., Wu, Y., Luo, H., Wang, M., and Xu, Y., *J. Catal.*, 2003, vol. 214, no. 1, p. 15.
15. Storozhenko, P.A., Svitsyn, R.A., Ketsko, V.A., Buryak, A.K., and Ul'yanov, A.V., *Russ. J. Inorg. Chem.*, 2005, vol. 50, no. 7, p. 980.
16. Simagina, V.I., Storozhenko, P.A., Netskina, O.V., Komova, O.V., Odegova, G.V., Larichev, Y.V., Ishchenko, A.V., and Ozerova, A.M., *Catal. Today*, 2008, vol. 138, nos, 3–4, p. 253.
17. Jiang, H.L., Singh, S.K., Yan, J.M., Zhang, X.B., and Xu, Q., *ChemSusChem*, 2010, vol. 3, no. 5, p. 541.
18. Patel, N., Fernandes, R., Guella, G., and Miotello, A., *Appl. Catal., B*, 2010, vol. 95, nos. 1–2, p. 137.
19. Tong, D.G., Zeng, X.L., Chu, W., Wang, D., and Wu, P., *J. Mater. Sci.*, 2010, vol. 45, no. 11, p. 2862.
20. Kalidindi, S.B., Indirani, M., and Jagirdar, B.R., *Inorg. Chem.*, 2008, vol. 47, no. 16, p. 7424.
21. Yan, J.M., Zhang, X.B., Shioyama, H., and Xu, Q., *J. Power Sources*, 2010, vol. 195, no. 4, p. 1091.
22. Hannauer, J., Demirci, U.B., Geantet, C., Herrmann, J.M., and Miele, P., *Phys. Chem. Chem. Phys.*, 2011, vol. 13, no. 9, p. 3809.
23. Cavaliere, S., Hannauer, J., Demirci, U.B., Akdim, O., and Miele, P., *Catal. Today*, 2011, vol. 170, no. 1, p. 3.
24. Kissinger, H.E., *Anal. Chem.*, 1957, vol. 29, no. 11, p. 1702.
25. Kim, J.H., Kim, K.T., Kang, Y.M., Kim, H.S., Song, M.S., Lee, Y.J., Lee, P.S., and Lee, J.Y., *J. Alloys Compd.*, 2004, vol. 379, nos. 1–2, p. 222.
26. Akdim, O., Demirci, U.B., and Miele, P., *Int. J. Hydrogen Energy*, 2011, vol. 36, no. 21, p. 13669.
27. Jun, L., Shuping, X., and Shiyang, G., *Spectrochim. Acta, Part A*, 1995, vol. 51, no. 4, p. 519.
28. Markova-Deneva, I., *J. Univ. Chem. Technol. Met.*, 2010, vol. 45, no. 4, p. 351.
29. Ozerova, A.M., Simagina, V.I., Komova, O.V., Netskina, O.V., Odegova, G.V., Bulavchenko, O.A., and Rudina, N.A., *J. Alloys Compd.*, 2012, vol. 513, no. 1, p. 266.
30. Andrieux, J., Swierczynski, D., Laversenne, L., Garron, A., Bennici, S., Goutaudier, C., Miele, P., Auroux, A., and Bonnetot, B., *Int. J. Hydrogen Energy*, 2009, vol. 34, no. 2, p. 938.
31. Santos, I.A., Eiras, J.A., Araújo, E.B., Sampaio, J.A., and Catunda, T., *J. Mater. Sci. Lett.*, 2011, vol. 20, no. 19, p. 1815.
32. Ma, L., Peng, Q., and He, D., *Catal. Lett.*, 2009, vol. 130, nos. 1–2, p. 137.
33. Hasegawa, R. and Ray, R., *J. Appl. Phys.*, 1979, vol. 50, no. 3, p. 1586.
34. Khan, Y., *J. Non-Cryst. Solids*, 1986, vol. 86, nos. 1–2, p. 137.
35. Zern, A., Kleinschroth, I., Gonzalez, A., Hernando, A., and Kronmüller, H., *J. Appl. Phys.*, 1999, vol. 85, no. 11, p. 7609.
36. Takahashi, M., Kim, C.O., Koshimura, M., and Suzuki, T., *Jpn. J. Appl. Phys.*, 1978, vol. 17, no. 10, p. 1911.